

Bayesian optimal reconstruction of the primordial power spectrum

M. Bridges*, F. Feroz, M.P. Hobson and A.N. Lasenby

Astrophysics Group, Cavendish Laboratory, JJ Thomson Avenue, Cambridge CB3 0HE, UK

Accepted —. Received —; in original form 23 August 2021

ABSTRACT

The form of the primordial power spectrum has the potential to differentiate strongly between competing models of perturbation generation in the early universe and so is of considerable importance. The recent release of five years of WMAP observations have confirmed the general picture of the primordial power spectrum as deviating slightly from scale invariance with a spectral tilt parameter of $n_s \sim 0.96$. Nonetheless, many attempts have been made to isolate further features such as breaks and cutoffs using a variety of methods, some employing more than ~ 10 varying parameters. In this paper we apply the robust technique of Bayesian model selection to reconstruct the *optimal* degree of structure in the spectrum. We model the spectrum simply and generically as piecewise linear in $\ln k$ between ‘nodes’ in k -space whose amplitudes are allowed to vary. The number of nodes and their k -space positions are chosen by the Bayesian evidence so that we can identify both the complexity and location of any detected features. Our optimal reconstruction contains, perhaps, surprisingly few features, the data preferring just three nodes. This reconstruction allows for a degree of scale dependence of the tilt with the ‘turn-over’ scale occurring around $k \sim 0.016 \text{ Mpc}^{-1}$. More structure is penalised by the evidence as over-fitting the data, so there is currently little point in attempting reconstructions that are more complex.

Key words: methods: data analysis – methods: statistical – cosmology: – cosmic microwave background

1 INTRODUCTION

The recent release by the Wilkinson Microwave Anisotropy Probe (WMAP) of five years of observations have confirmed that the primordial spectrum of density perturbations is consistent with being purely adiabatic and *close* to scale invariant, in perfect harmony with the simplest inflationary scenarios. This agreement appears remarkably robust when extended to independent datasets such as measures of the matter power spectrum from galaxy redshift surveys (Tegmark et al. 2006). Alternative models of the spectrum containing various features have been considered. These include an exponential large scale cutoff (Efstathiou 2003a) to explain the quadrupole power decrement, and theoretically motivated spectra to model the inflationary potential (Nicholson & Contaldi 2008) or account for discontinuities from early universe phase transitions (Barriga et al. 2001). Reconstructions of the spectrum, limiting *a priori* assumptions about its structure, have typically involved fitting some basis functions, such as wavelets (Mukherjee & Wang 2003), some deconvolution method (Shafieloo & Souradeep 2004; Tocchini-Valentini et al. 2005) or directly ‘binning’ the spectrum into an arbitrary number of band powers (Bridle et al. 2003). However, most previous methods fail to account for Occam’s razor since they assume that more complexity, and typically more ‘detected’

features, are necessarily important in explaining the data. Recently Verde & Peiris (2008) reconstructed the spectrum, while minimising the level of complexity needed via a cross-validation with a ‘hold-out’ portion of the data. This approach is a timely progression, but in this paper we attempt a more statistically robust procedure with an optimal reconstruction using the Bayesian evidence to decide how much detail one should fit and where it is located in k -space, based solely on the data.

2 PARAMETERISATION OF THE PRIMORDIAL SPECTRUM

Inflationary models generically predict the initial spectrum of scalar density perturbations to be close to scale invariant with just slight scale dependence, commonly called *tilt*, a red (blue) tilt for decreasing (increasing) amplitude at smaller scales. Theoretical motivation for this form is found in the slow-roll formulation of inflation. Previous studies (e.g. Leach et al. 2002 & Peiris & Easther 2006) have used spectral models defined explicitly by the physical slow-roll parameters but here we define the spectrum essentially empirically using a spectral amplitude, A_s , a spectral index or tilt parameter n_s and a *running* parameter $n_{\text{run}} \equiv \frac{dn_s}{d \ln k}$ denoting any

* E-mail: m.bridges@mrao.cam.ac.uk

Table 1. Priors of the base cosmological parameters.

$0.018 \leq \Omega_b h^2 \leq 0.032$
$0.04 \leq \Omega_{dm} h^2 \leq 0.16$
$0.98 \leq \Theta \leq 1.1$
$0.01 \leq \tau \leq 0.5$
$-0.1 \leq \Omega_k \leq 0.1$

tilt scale dependence:

$$\mathcal{P}(k) = A_s \left(\frac{k}{k_0} \right)^{n_s - 1 + \frac{1}{2} \ln \left(\frac{k}{k_0} \right) n_{\text{run}}}, \quad (1)$$

where k_0 denotes the scale about which the tilted spectrum pivots which throughout we set at 0.05 Mpc^{-1} . It has been shown previously (Trotta 2007) that this parameterisation, although not physical in itself, does within suitable prior ranges adequately model the inflationary primordial spectrum.

The parameterisation described by Eqn. 1 encompasses the most commonly tested power spectra, namely: the scale invariant or Harrison-Zel'dovich spectrum (in which $1 - n_s = n_{\text{run}} = 0$), the tilted spectrum ($n_{\text{run}} = 0$) and a running spectrum in which the tilt becomes a function of scale ($n_{\text{run}} \neq 0$). To these we can add a ‘cutoff’ spectrum which allows $\mathcal{P}(k)$ to drop to zero below some variable cutoff scale and above which behaves like a tilted spectrum. We shall use this as a simple test as to whether the addition of some cutoff feature is actually required by the data.

In this paper, however, we are primarily interested in determining structure in the primordial spectrum using an optimal model-free reconstruction. We use the Bayesian evidence as discriminator in fitting a simple spectrum based on linear interpolation between a set of amplitude-varying *nodes* in k -space. This is essentially the same *binning* format as that used previously by a number of authors (Bridle et al. 2003, Bridges et al. 2006, Bridges et al. 2007, Spergel & et al. 2007) however here we aim to allow the data to decide upon the location *and* number of nodes via the evidence.

In the background cosmology we allow the possibility of a non-flat Λ CDM cosmology specified by the following five parameters: the physical baryonic matter density $\Omega_b h^2$, the physical dark matter density $\Omega_{dm} h^2$, the ratio of the sound horizon to angular diameter distance Θ , the optical depth to reionisation τ and the curvature density Ω_k , where the corresponding priors are listed in Table 1. Additionally we allow a contribution to the small-scale power in the CMB spectrum from Sunyaev-Zeldovich fluctuations as performed in the WMAP analysis (Dunkley et al. 2008, Komatsu et al. 2008).

The structure of the paper is as follows: in section 3 we describe basic model selection and our algorithm, in section 4 we list the individual datasets and discuss the combinations used, in section 5 we will review the current status of the standard, scale-invariant, tilted and running parameterisations of the power spectrum in light of the WMAP5 data and test the possibility of a large-scale cutoff. We then briefly discuss the consistency of the datasets using a quantifiable Bayesian measure in section 6. The remainder of the paper is then devoted to our optimal reconstruction (section 7) and our conclusions (section 8).

3 BAYESIAN INFERENCE

The Bayesian methodology provides a logical and consistent approach to extracting inferences from a set of data. Given a model,

or hypothesis H defined by a set of parameters Θ , Bayes’ theorem tell us how to determine the probability distribution of those parameters given the data \mathbf{D} :

$$\Pr(\Theta|\mathbf{D}, H) = \frac{\Pr(\mathbf{D}|\Theta, H) \Pr(\Theta|H)}{\Pr(\mathbf{D}|H)}, \quad (2)$$

where for future simplicity we define $\Pr(\Theta|\mathbf{D}, H) \equiv P(\Theta)$ as the posterior probability distribution of the parameters, $\Pr(\mathbf{D}|\Theta, H) \equiv \mathcal{L}(\Theta)$ as the data likelihood, and $\Pr(\Theta|H) \equiv \pi(\Theta)$ as the prior. Of particular importance here is the Bayesian evidence term $\Pr(\mathbf{D}|H) \equiv \mathcal{Z}$.

To obtain parameter constraints given a model the evidence is often ignored since it is independent of the parameters Θ . The posterior distribution is simply constructed by Monte Carlo sampling from the combined distribution $P(\Theta) \propto \mathcal{L}(\Theta)\pi(\Theta)$. Typically most of the posterior *weight* lies in a relatively small range of Θ and so using some importance sampling procedure, like Metropolis-Hastings, one quickly generates estimates of the best-fitting parameter values and their variances.

Bayesian model selection also relies on the posterior distribution and is based on its *normalisation* over the parameter space Θ . This term is in fact given by the evidence \mathcal{Z} and can be computed by performing the integral:

$$\mathcal{Z} = \int \mathcal{L}(\Theta)\pi(\Theta)d^N \Theta, \quad (3)$$

where N is the dimensionality of the parameter space. Thus \mathcal{Z} can be defined as the average of the likelihood over the prior. The evidence naturally incorporates Occam’s razor: a simpler theory with a more compact parameter space will have a larger evidence than a more complicated one, unless the latter is significantly better at explaining the data.

The question of which model best describes the data can then be addressed by comparing the properly normalised posterior probability distributions calculated for two hypotheses H_0 and H_1 .

$$\frac{\Pr(H_1|\mathbf{D})}{\Pr(H_0|\mathbf{D})} = \frac{\Pr(\mathbf{D}|H_1) \Pr(H_1)}{\Pr(\mathbf{D}|H_0) \Pr(H_0)} = \frac{\mathcal{Z}_1 \Pr(H_1)}{\mathcal{Z}_0 \Pr(H_0)}, \quad (4)$$

where $\Pr(H_1)/\Pr(H_0)$ is the a priori probability ratio for the two models, which can be set to unity if we have no reason to prefer hypothesis H_0 over H_1 initially. For convenience the ratio of evidences $\mathcal{Z}_1/\mathcal{Z}_0$ (or equivalently the difference in log evidences $\ln \mathcal{Z}_1 - \ln \mathcal{Z}_0$) is often termed the *Bayes’ factor* \mathcal{B}_{01} . Interpreting the level of significance one should ascribe to a given \mathcal{B} value is often a matter of experienced judgement, however a suitable guideline scale has been laid out by Jeffreys (1961). If $\mathcal{B} < 1$ H_1 should not be favoured over H_0 , $1 < \mathcal{B} < 2.5$ is significant, $2.5 < \mathcal{B} < 5$ is strong evidence while $\mathcal{B} > 5$ would be considered decisive.

Computation of the multidimensional integral Eqn. 3 is not a trivial task and approaches such as thermodynamic integration have previously been shown to be both slow and inaccurate. In this analysis we apply the method of nested sampling (Skilling 2004) which transforms the N -dimensional integral in Eqn. 3 to one dimension and computes it by drawing uniform samples from ever decreasing nested *shells* in the prior parameter space. We apply an algorithm based on this procedure called MULTINEST which constrains the nested shells in the prior space with N -dimensional ellipsoids (Feroz & Hobson 2008; Feroz et al. 2008). This approach results in an order of magnitude improvement in efficiency and accuracy over previous methods.

4 DATASETS CONSIDERED

In this analysis we have divided the data into two categories: CMB only and CMB plus observations of the matter power spectra from Large Scale Structure (LSS) surveys. This is primarily designed so that we can test consistency across the datasets in an initial analysis before carrying over a final set of data to our power spectrum reconstruction. We consider a number of CMB experiments including the latest five year release from WMAP (Hinshaw et al. 2008) plus recent results from the Arcminute Cosmology Bolometer Array [ACBAR; Reichardt et al. 2008] which should be uniquely useful here due to their tight constraints out to small angular scales. In addition we include Cosmic Background Imager observations [CBI; CBI Supplementary Data 2004; Readhead et al. 2004] and Balloon Observations of Millimetric Extra-galactic Radiation and Geophysics [BOOMERANG; Piacentini et al. 2006; Jones et al. 2006; Montroy et al. 2006]. LSS data includes the luminous red galaxy (LRG) subset D4 of the Sloan Digital Sky Survey [SDSS; Tegmark et al. 2004] and the two degree field survey [2dF; Cole et al. 2005]. We allow for modelling of non-linearities and galaxy biasing of the matter power spectrum in the LRG sample using the transfer function defined by Cole et al. (2005)¹. We analytically marginalise over the parameter combination Qb^2 and set $A = 1.4$, as shown by Cole et al. (2005) to be adequate.

5 SIMPLE POWER SPECTRUM MODELS

Many previous analyses have considered the four most basic parameterisations described in Section 2 in light of WMAP observations plus a plethora of higher resolution CMB and Large Scale Structure (LSS) data. Here we will briefly summarise the current status of these models. The first year WMAP [WMAP1] data on its own had no preference for a tilt ($n_s = 0.99 \pm 0.04$) but the inclusion of higher resolution CMB data and LSS data induced a marked red-tilt (Spergel et al. 2003). By year three of WMAP [WMAP3], with tighter constraints on the second and third acoustic peaks, a red tilt became discernible even without additional datasets (Spergel & et al. 2007) $n_s = 0.958 \pm 0.016$. The recent WMAP five year release confirms the value at ~ 0.96 with a mean estimate of 0.963 ± 0.015 (Komatsu et al. 2008). The position of a running spectral index has been more controversial: WMAP1 alone preferred a large mean value of n_{run} though with little statistical significance, with WMAP3 alone however a value of n_{run} was found, that within 1σ limits was deviant from zero. A number of authors (Viel et al. 2006; Seljak et al. 2006; Bridges et al. 2007) have subsequently found that in the case of WMAP3, running was almost completely removed on addition of the SDSS Ly- α forest data (McDonald et al. 2006). Ly- α data probes scales (\sim Mpc), small in comparison to other datasets used, and so provides a long ‘lever arm’ for primordial spectrum analyses. However further discrepancies in other cosmological parameters, at the level of almost 2σ , has cast some doubt on the conclusions made when using this data so we do not include it here.

Theoretically motivated priors on the tilt are easily extracted from the slow-roll inflationary framework as $n_s = 1 - 6\epsilon + 2\eta$, where ϵ and η are the slow-roll parameters. For the slow-roll conditions to be met we then require that $\epsilon \sim 0$ and that $\eta \ll 1$. If we assume that η must be ≤ 0.1 we get $n_s = 1 \pm 0.2$ (Trotta

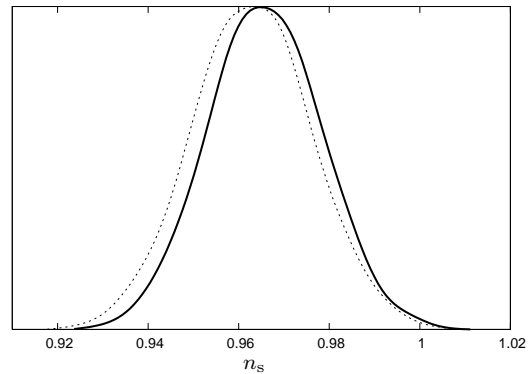


Figure 1. Marginalised posterior probability of the spectral tilt n_s using CMB plus LSS data (solid) and CMB data alone (dotted). Note: in this and all subsequent figures each posterior is normalised independently.

2007). Spectral running is expected to be small, in fact n_{run} even at the level of 0.05 would rule out all simple inflationary scenarios (Easter & Peiris 2006). Thus if assuming slow-roll inflation we are free to set quite a tight prior $-0.2 \leq n_{\text{run}} \leq 0.2$. Uniform prior distributions over these ranges were adopted throughout.

Using MULTINEST as described in section 3 a set of posterior samples and model evidences were computed using the two basic datasets described in section 4 for the basic suite of models: H-Z spectrum, a tilted spectrum, a tilted spectrum with running and a tilted spectrum with a large scale cutoff. For now this simply serves as a useful sanity check for consistency between datasets, but later, in section 6 the appropriate Bayesian consistency measure will be applied to quantify any discrepancy.

We will now discuss the most common set of parameters that are typically used to describe the primordial spectrum: n_s from the tilted spectrum and n_{run} from the tilted spectrum with running. Figure 1 shows the marginalised posterior distribution on n_s from the tilted power spectrum using CMB data alone and in a joint analysis with LSS data. We find a mean value of $n_s = 0.962 \pm 0.018$, this value shifting upwards only marginally when including LSS ($n_s = 0.967$). These results are in good agreement with Komatsu et al. (2008) despite our relaxation of the requirement for universal flatness. Deviations from $n_s \approx 1$ such as these, at $\sim 2\sigma$ are now seen as persuasive evidence for a red-tilt. The Bayesian evidence however would need a significantly larger deviation (in fact closer to the level of 5σ !) to conclude decisively that tilt was present. At present these results produce a Bayes’ factor of $\mathcal{B}_{H-Z, n_s} \sim 1.1 - 1.6$ (see Table 2), that is significant but certainly not strong evidence in favour of a tilt. Running in the spectrum remains ambiguous with CMB data alone (roughly a 1σ deviation from $n_{\text{run}} = 0$), but the addition of LSS data shifts the mean value to within ± 0.02 of zero (Fig. 2). This effect has been observed on a number of occasions (e.g. Tegmark et al. 2003, Bridges et al. 2007) and is due mainly to the excellent high- k constraints coming from the LRG data. The evidence does not favour running in either dataset, with $|\mathcal{B}_{H-Z, n_{\text{run}}} \sim 0.4|$, just outside our estimated margin of error.

Figure 3 shows the measured C_ℓ values at low- ℓ for WMAP1, 3 and 5 with the best-fit theoretical model (and corresponding cosmic variance limits) as determined by Dunkley et al. (2008). The mean C_ℓ estimators at both the quadrupole and octopole in WMAP1 are seen to be deviant from the fiducial model by close

¹ $P_{\text{Non-linear}}(k) = b^2 \frac{1+Qk^2}{1+Ak^2} P_{\text{Linear}}(k)$

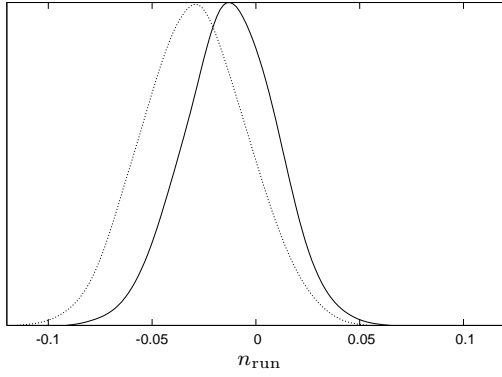


Figure 2. Marginalised posterior probability of spectral running n_{run} using CMB plus LSS data (solid) and CMB data alone (dotted).

Table 2. Bayes' factors comparing a scale invariant (H-Z) spectrum with models containing tilt, running and a large scale cutoff using both CMB alone and CMB + LSS data.

Model	CMB	CMB + LSS
H-Z	0.0 ± 0.3	0.0 ± 0.3
n_s	$+1.6 \pm 0.3$	$+1.1 \pm 0.3$
n_{run}	$+0.4 \pm 0.3$	-0.4 ± 0.3
k_c	$+1.5 \pm 0.3$	$+1.3 \pm 0.3$

to the cosmic variance limit. The situation changed somewhat in the three-year (and subsequently five-year) release so that now the octopole has shifted upwards to lie comfortably close to its expected value, but the quadrupole remains anomalously low. The statistical significance has been questioned by many authors (e.g. Efstathiou 2003b) and spurious alignments between the affected multipoles have been suggested as evidence of some large scale foreground contamination (de Oliveira-Costa et al. 2004). However here we shall assume that the effect is a real one and attempt to explain the large-scale CMB decrement with a feature in the primordial spectrum.

Naturally, at present the data will prefer a model that includes a large scale cutoff, but does the data find one *necessary*? We can test this with a simple ‘cartoon’ model by abruptly curtailing a tilted spectrum below some variable scale k_c so that its form is given by:

$$\mathcal{P}(k) = \begin{cases} 0, & k < k_c \\ A_s \left(\frac{k}{k_0}\right)^{n_s-1}, & k \geq k_c \end{cases} \quad (5)$$

The marginalised posterior distributions for k_c in Fig. 4 show a preferred scale around $2.7 \times 10^{-4} \text{ Mpc}^{-1}$, consistent with an angular scale around $\ell = 2 - 4$ as expected. Interestingly although blind to scales around the cutoff, a joint analyses with LSS data shows a pronounced peak at $k_c \approx 0$ suggesting that the constraining power of, particularly LRG data, now matches current CMB data. In other words, now that constraints at smaller scales are becoming tighter, anomalies such as the cutoff are becoming less important. The evidence confirms this (see Table 2) showing that the extra parameter is superfluous.

The current position of these standard parameterisations then appears straightforward, with CMB data alone and in joint analysis with LSS, a purely scale-invariant spectrum is significantly disfavoured by the data. However the addition of a running parameter remains of dubious necessity with CMB data alone and is actually

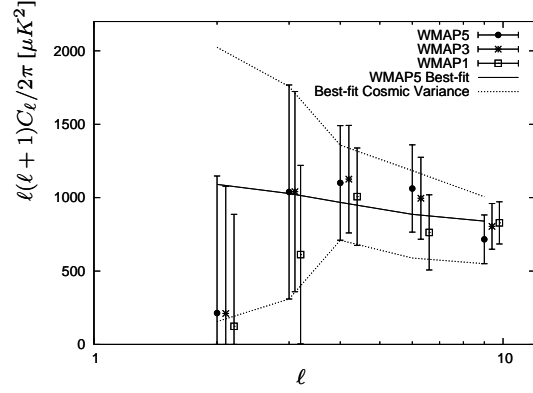


Figure 3. Low- ℓ multipoles and 1σ error bars from three releases of WMAP data the best-fit fiducial power spectrum based on WMAP5 inferences is also plotted and shows the associated cosmic variance limits. [Note ℓ values are slightly offset for clarity.]

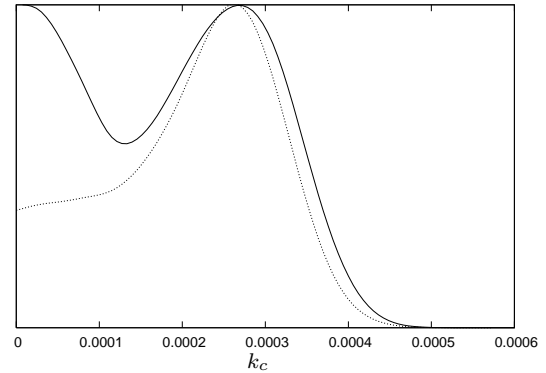


Figure 4. Marginalised posterior probability of the large scale spectral cutoff k_c using CMB plus LSS data (solid) and CMB data alone (dotted).

disfavoured when LSS constraints are included. A large scale cut-off in the primordial spectrum remains a suitable explanation of the WMAP quadrupole decrement but according to the evidence there is currently no need to include it in the model.

6 DATASET CONSISTENCY

Combining multiple datasets in joint analyses, in particular the recent inclusion of observations of the baryonic acoustic oscillations in LSS surveys with CMB observations, have led to tight constraints on the cosmological parameters (Tegmark et al. 2006). Authors regularly comment on the relative consistency between datasets by comparing the parameter constraints made with each set individually and when combined, however little effort is normally made to quantify this consistency. Marshall et al. (2006) established just such a method using the Bayesian evidence (see also Hobson et al. 2002). This is important for our reconstruction as experimental features, such as discontinuities on scales where observations meet may result in false detections of spectral structure. The two datasets chosen, CMB and LSS, now overlap considerably on scales starting around $k \sim 0.02 \text{ Mpc}^{-1}$. If a data inconsistency were to exist it would likely appear as a feature close to this scale. Curiously such a feature has been identified, Verde et al. (2003) detected a deviation from a simple tilt around $k \sim 0.01$

Table 3. Bayes’ factors comparing the assumption of dataset consistency ($H_0 = \text{consistent}$, $H_1 = \text{inconsistent}$) using CMB + LSS datasets for each of the models considered above.

Model	\mathcal{B}_{01}
H-Z	$+2.6 \pm 0.3$
n_s	$+1.9 \pm 0.3$
n_{run}	$+1.1 \pm 0.3$
k_c	$+1.5 \pm 0.3$

Mpc^{-1} . This effect was strongest when using WMAP data alone, appearing considerably reduced in joint analyses with other higher resolution CMB and LSS data. Here we will apply a Bayesian consistency check to assess whether we can be justified in combining these datasets in our analyses.

Consider the null hypothesis H_0 that given two independent sets of data there is one model and one set of parameters to explain them. In this case we would say that the datasets are ‘consistent’. However we would really like a quantitative measure by which to assess this consistency. If we consider the alternative, H_1 , that each dataset separately prefers a different set of parameters, we can then construct the Bayes’ factor between the two hypotheses as:

$$\mathcal{B}_{01} \equiv \frac{\Pr(\mathbf{D}|H_0)}{\Pr(\mathbf{D}|H_1)} \quad (6)$$

$$= \frac{\mathcal{Z}_0(\mathbf{D})}{\prod_i \mathcal{Z}_1(\mathbf{D}_i)} \quad (7)$$

where we have written $\Pr(\mathbf{D}|H_1)$ as the product of evidences from each individual (independent) dataset D_i . In this form consistency can easily be checked by computing the joint evidence and the evidence due to each dataset separately. As with any other hypothesis test we can assess the appropriate model with the aid of the Jeffreys’ scale based on the final Bayes’ factor.

Table 3 lists the appropriate Bayes’ factors for each model based on our two datasets: CMB and CMB+LSS. Firstly, all factors are positive and greater than unity, confirming that these sets of data are indeed all essentially free from discrepancies. On the Jeffreys’ scale, hypothesis H_0 that the datasets are consistent, is favoured *significantly*. The highest degree of consistency occurs for the H-Z model, this is not surprising as both datasets provide equivalent constraints on the amplitude of fluctuations. Where we did observe differences in parameter constraints with the running and cutoff models, we can see how this measure has quantified the discrepancy. For instance, the addition of LSS data, led to slightly tighter constraints on the parameter n_{run} (as well as being pulled closer to zero) (Fig. 5) and this difference has lowered the evidence in favour of consistency from nearly two log units to ~ 1 . A similar but less pronounced effect is observed with the cutoff model.

The deviations seen are minor. The worst discrepancy found, using the running model, was still consistent with CMB data, with odds of around 3:1 in favour (i.e. $e^{\Delta \ln \mathcal{Z}} = e^{\mathcal{B}_{01}}$) while under the assumption of scale invariance the datasets are consistent at around 14:1 in favour. These differences are best explained by the superior small scale constraints that are possible when using LSS data rather than a genuine inconsistency, and we feel it is justified to perform our reconstruction using the joint set of data given the increased constraining power possible.

7 OPTIMAL POWER SPECTRUM RECONSTRUCTION

The degree of structure that can or should be usefully constrained in the primordial spectrum has been a source of increasing debate in the literature. Recently Verde & Peiris (2008) applied a smoothing spline technique (Sealfon et al. 2005) that attempts, via cross-validation with part of the data, to minimise the complexity of the parameterisation. This approach selects an initial set of ‘knots’ that are fixed in k space but whose amplitudes may vary, and through which various splines are fitted, thus constructing the primordial spectrum. This approach will preferentially identify smooth structures rather than sharp breaks, and while it is true that most deviations from scale invariance given the slow-roll assumption will be smooth, we do not believe the data is currently accurate enough for this to be the limiting factor for an analysis. We have thus attempted to use the simplest reconstruction possible, while still maintaining continuity, by linearly interpolating between a set of *nodes*, at which we allow the amplitude to vary. Our reconstructions gain complexity by the addition of new nodes and on estimating the evidence for each reconstruction one can decide exactly the level of parameterisation deemed necessary by the data.

We start with one node, see Fig. 5 (a), so our base model is equivalent to the scale-invariant H-Z spectrum. The next model, (b) allows for two, sufficiently separated, independently varying nodes, thus emulating a tilted spectrum. We then add a third node (c), spaced logarithmically midway between two existing nodes. This process continues, at each stage the additional node being added between the existing ones, so that at the fourth stage there are two possibilities, (d) and (e). At the fifth stage there are three possibilities, at the sixth, four and so on. One can see that by such a process, using the evidence as the model discriminator at each stage, not only are the number of parameters constrained but also the location of features in k -space, so that we can faithfully reconstruct *both* the degree and position of any spectral structure. It should also be clear that if we *branch* at one reconstruction by accepting a new node at some position (say the lower k node in (d) rather than (e)), we still retain the option of splitting the unaccepted region later (i.e. in (h)). Thus we fully explore the options in feature space and should hierarchically detect as much structure as the data will allow.

The only assumptions required are the positions of the two extremal nodes, k_{min} and k_{max} . These bounds were chosen to lie at sufficiently large ($k_{\text{max}} = 2.7 \text{ Mpc}^{-1}$) and small ($k_{\text{min}} = 0.0001 \text{ Mpc}^{-1}$) scales so as safely to encompass all current observational probes *and* crucially, when more than 2 nodes are used, to allow the spectrum to tend *naturally* to zero power, particularly on small scales. A conservative amplitude prior of 0.55×10^{-10} was used throughout on all nodes.

7.1 Model Comparison I: the Bayesian evidence

The marginalised 1-dimensional posterior distributions for the amplitude at each node and for each reconstruction are shown in Fig. 6 [Fig. 5 illustrates the corresponding form of the reconstructed spectra from the mean posterior estimates (with 1σ error bars on the amplitudes)]. Comparing figure (b) in both Figs. 5 and 6 we see that there is only an upper bound on the amplitude at k_{max} , with no lower bound. This is a consequence of our choice of a large k_{max} , well above any current experimental constraint and simply allows the power to gradually fall to zero. The difference in evidence is minimal between the base and two node model with $\mathcal{B}_{12} = 0.66$ being too small, on the Jeffreys’ scale to draw any decisive conclusions, though within the error the evidence marginally prefers

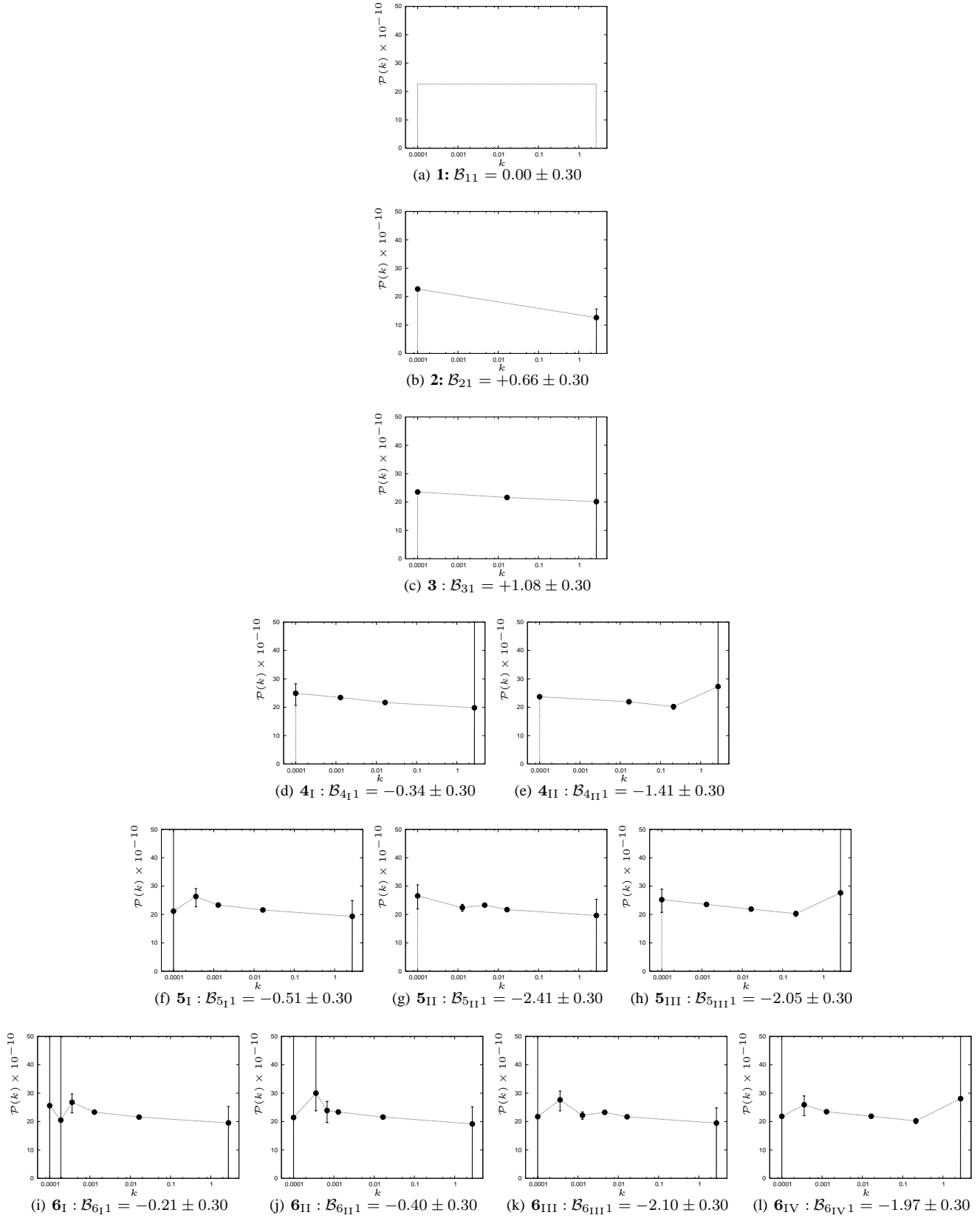


Figure 5. Linear interpolated reconstructions of the primordial spectrum with associated Bayes' factors with respect model 1. The amplitude was allowed to vary at each of the nodes (shown with black circles). Mean amplitude values and 1σ limits are shown, taken from the posteriors illustrated in Fig. 6.

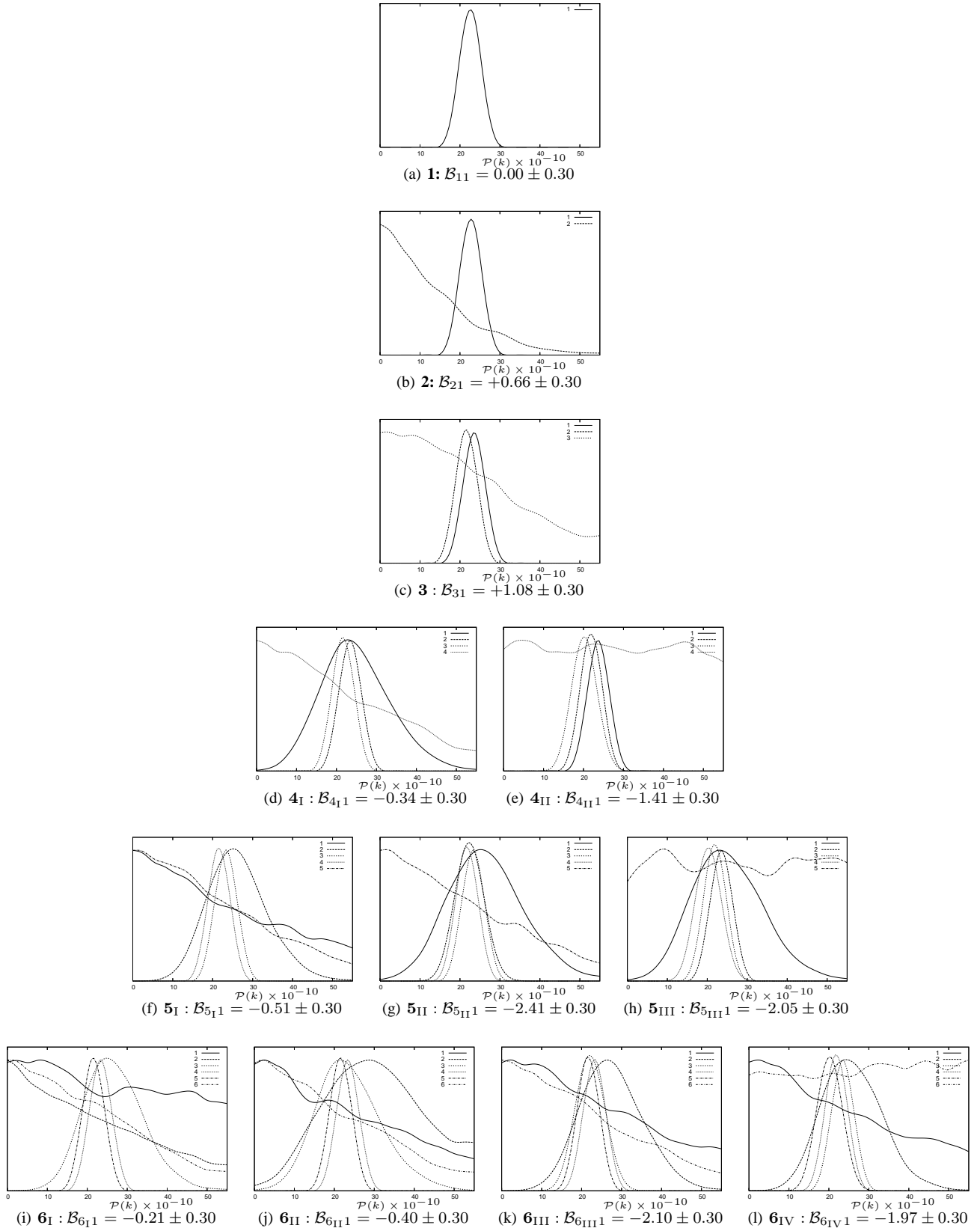


Figure 6. Marginalised 1-dimensional posterior distributions of the amplitude at each k -space node used in each reconstruction.

model 2. The third model adds a node at $k \sim 0.0166 \text{ Mpc}^{-1}$ emulating a degree of spectral running by allowing a slight variation in the interpolated slopes between the three nodes. Though no meaningful constraint is possible at the upper k scale, this model is preferred over model 2 with $\mathcal{B}_{23} \sim 0.4$ and significantly over the base model by $\mathcal{B}_{02} \sim 1.1$ units. The fourth stage reconstruction requires us to test two combinations of node positions, the first, 4_{I} , splits the lowest k bin at $k \sim 0.00129 \text{ Mpc}^{-1}$ while the second, 4_{II} divides the upper k bin. $\mathcal{B}_{34_{\text{I}}}$ and $\mathcal{B}_{34_{\text{II}}}$ both significantly disfavour the addition of a fourth node. This result points to some deviation from scale invariance at around the position $k \sim 0.01$, the rough location of the additional node in model 3. Further parameterisation both above (4_{II}) and below (4_{I}) this scale is disfavoured, lending credence to the general conclusions of Verde & Peiris (2008) who found a similar ‘turn-over’ scale. According to the evidence the optimal reconstruction contains, perhaps surprisingly only three parameters.

It is interesting to note that the parameterisation in 4_{I} is significantly preferred over 4_{II} , i.e. an additional node seems to be preferred on large scales over small. Although technically redundant we can continue to a fifth and sixth stage to see if this effect continues. Assuming then that the fourth stage evidence has now indicated a preference for large scale (small k) structure over small we continue by sub-dividing the largest k bin of 4_{I} again at $k \sim 0.00036$, which we denote as 5_{I} . The two other possible splittings being 5_{II} at $k \sim 0.00462$ and 5_{III} at $k \sim 0.21$. To within estimated error $\mathcal{B}_{4_{\text{I}}5_{\text{I}}} \sim 0$ and again both 5_{II} and 5_{III} are significantly disfavoured. This result is repeated at the sixth stage.

So, curiously, although the evidence peaks at model 3 there is a substantial preference in all subsequent reconstructions for additional amplitude nodes to be placed at large scales (i.e. models 4_{I} , 5_{I} and 6_{I}). Furthermore the evidence is observed to *plateau* in value with $\mathcal{B}_{4_{\text{I}}5_{\text{I}}}$ and $\mathcal{B}_{5_{\text{I}}6_{\text{I}}}$ being roughly zero. The first result could suggest that although the data cannot yet cope with the extra complexity, large scale structure is useful in a model. However when combined with the second result this points to the additional parameters not *over complicating* the model but instead being *ignored* and left unconstrained by the data. The evidence is quite deliberately adept at ignoring such extra complexity; the extra undetermined parameter direction simply does not affect the average posterior over the prior. This effect is demonstrated here by comparing Figures 5 (d) and (f) where the act of placing an additional node at $\sim 0.00129 \text{ Mpc}^{-1}$ removes all constraint on the amplitude at node k_{min} and thus *de-facto* removes a parameter from the analysis. To account correctly for this effect, the analyst requires a further level of model discrimination, that can interpret quantitatively the constraining power of a given model and data combination. For this we must fully define what we are penalising in extra model complexity, and for this we turn to the Bayesian *complexity*.

7.2 Model Comparison II: the Bayesian complexity

The advantage of Bayesian model selection is that it penalises model parameters that cannot be justified by the data. However the number of free parameters is only the most naive measure of the complexity of a model. A more thorough comparison can be gleaned from what is termed the Bayesian or *effective* complexity of a model. This definition was first given by Spiegelhalter et al. (2002) and was subsequently introduced into cosmology by Kunz et al. (2006). The starting point is a quantifiable definition of how a set of data can improve the prior knowledge of a model. In other words a measure of the relative difference

between the posterior and prior distributions, sometimes termed the *information gain*. The Kullback-Leibler (KL) divergence D_{KL} measures just this, via the relative entropy between two probability distributions, P and π :

$$D_{\text{KL}}(P, \pi) \equiv \int P(\Theta|\mathbf{D}) \ln \frac{P(\Theta|\mathbf{D})}{\pi(\Theta)} d\Theta. \quad (8)$$

From this definition the Bayesian complexity can then be defined as the difference in D_{KL} between some real experiment and the ideal situation where the information gain is maximised. To see how this works, let us take the ideal example of a uniform prior distribution π and an excellent set of data \mathbf{D} such that on completion of a Bayesian analysis the prior distribution collapses into a δ -function posterior distribution about some parameter vector Θ' . This we take as our *ideal* scenario in which the divergence between posterior and prior is maximised and is given approximately by $D'_{\text{KL}} = \ln P(\Theta')/\pi(\Theta')$. In a realistic experiment of course the posterior $P(\Theta)$ will resemble some (approximately) multidimensional Gaussian distribution with some mean $\hat{\Theta}$ parameter vector and an associated variance so that the divergence would be given simply by Eqn. 8. The Bayesian complexity C_{B} can thus be defined as the difference between the ideal point estimate D'_{KL} and the actual divergence:

$$C_{\text{B}} \equiv -2 \left(D_{\text{KL}}(P, \pi) - \widehat{D_{\text{KL}}} \right). \quad (9)$$

This leaves us free to choose an appropriate point estimate that maximises information gain -which for most well constrained cosmological problems can be taken to be the *mean* of the full posterior distribution. Using Eqn. 8 and Bayes’ theorem one can rewrite Eqn. 9 as:

$$C_{\text{B}} \equiv -2 \int P(\Theta|\mathbf{D}) \ln \mathcal{L}(\Theta) + 2 \ln \mathcal{L}(\hat{\Theta}) d\Theta. \quad (10)$$

By defining an effective χ^2 through $\mathcal{L}(\Theta) \propto e^{-\chi^2/2}$, such that all constant factors within the likelihoods drop out, we can define the Bayesian complexity as:

$$C_{\text{B}} = \overline{\chi^2(\Theta)} - \chi^2(\bar{\Theta}), \quad (11)$$

where the first term denotes the mean χ^2 across a set of posterior samples while the second term is the χ^2 at the mean parameter values.

Based on this definition the Bayesian complexity succinctly compares the *constraining power* of the data with the *predictivity* of the model. Thus a model with highly restrictive priors, and unconstrained posteriors will have a *low* Bayesian complexity, as the predictiveness of the model was already very high initially. Conversely, wide priors with highly constrained posteriors will result in a *high* complexity (which can tend to a maximal value equal to the *actual* number of model parameters, C_0) as the data constrained the model substantially over the uninformative priors.

It should be emphasised that estimates of the Bayesian complexity cannot be used in isolation for model selection, blindly choosing the model with the smallest complexity would simply *under-fit* the data. Instead it provides a useful discriminator in cases where the evidence difference between models is so small (say < 1 log unit on the Jeffreys’ scale) that little inference can be drawn with the evidence alone. Besides the most obvious scenario, where both models are essentially equally informative, the case, as we had in the last section can be envisaged where additional parameters are simply left unconstrained by the data, such that in the evidence integral this direction is simply *averaged over*. Here the complexity can quantify whether or not the additional parameters have actually

Table 4. The reconstruction Bayesian complexity C_B and actual number of model parameters C_0 .

Model	C_0	C_B
1	7	5.35 ± 0.10
2	8	6.35 ± 0.10
3	9	7.03 ± 0.10
4 _I	10	7.82 ± 0.10
4 _{II}	10	7.18 ± 0.10
5 _I	11	8.04 ± 0.10
5 _{II}	11	8.60 ± 0.10
5 _{III}	11	8.37 ± 0.10
6 _I	12	8.04 ± 0.10
6 _{II}	12	8.60 ± 0.10
6 _{III}	12	8.37 ± 0.10
6 _{IV}	12	8.37 ± 0.10

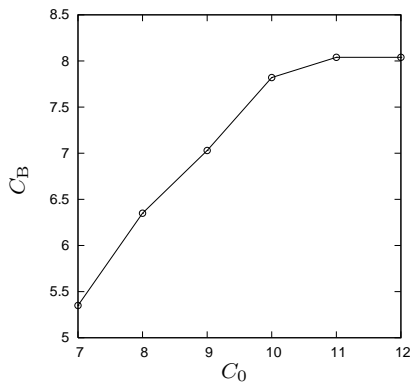


Figure 7. Bayesian complexity C_B versus actual number of model parameters C_0 for models: 1, 2, 3, 4_I, 5_I and 6_I. Note how C_B increases almost linearly with C_0 until model 4_I ($C_0 = 10$) when C_B begins to plateau in value as successively less well constrained parameters are added.

been constrained and thus extracted any further information from the data.

Table 4 lists the recovered complexity for each of our reconstructions tested. It should be noted that we have chosen quite a generic background cosmology accounting for both the possibility of spatial curvature, via the Ω_k parameter and the marginalisation over a possible SZ contribution at high ℓ as was done in Komatsu et al. (2008). Inclusion of recent LRG data with their associated tight constraints on Ω_k will minimise any effect on C_B , however A_{SZ} remains essentially unconstrained by current data. Thus it is not surprising to see our base, scale invariant model 1 having an effective complexity significantly less than C_0 . This need not concern us here however, as we are primarily interested in the relative difference of C_B as we increase the reconstruction complexity.

Since the evidence is maximised for model 3, this should be our preferred parameterisation. Of course the Bayes' factor \mathcal{B}_{32} between models 3 and 2 is only ~ 0.4 , or on the Jeffreys scale of little significance, and since the Bayesian complexity for model 2 is significantly smaller (by ~ 0.7) than 3 should we then argue that model 2 should in fact be preferred? Looking at the marginalised posteriors of 3, the fact that it is preferred is not at all surprising, as the addition of the node at $k \sim 0.01656 \text{ Mpc}^{-1}$ leaves no amplitude constraint at k_{max} . In effect the evidence is maximised for

model 3 as it is a *de-facto* two parameter model. However crucially it provides the required tilt over a k range that is well constrained by data *and* allows a deviation in this tilt above $k \sim 0.01$. Further modelling of the upper tilt, via say an extra node as we performed in model 4_{II} was strongly disfavoured $\mathcal{B}_{34II} \sim 2.5$. So the inclusion of complexity in the analysis has not altered our general conclusions, as the evidence difference between models 2 and 3 is minimal, it simply serves to highlight the lack of significance placed by the data in anything other than a tilted spectrum at present.

The complexity can further explain the degeneracy in evidence values for those models where we introduced additional large scale structure (e.g. 4_I, 5_I and 6_I). Fig. 7 plots C_B against C_0 for these models (and for comparison the first three models). As we increase the number of parameters in going from model 1 to 3 the Bayesian complexity is seen to rise roughly linearly, from which we infer that the data can usefully constrain all of the model parameters and thus can warrant the additional parameterisation. This trend continues to model 4_I, but thereafter C_B tends rapidly to a constant value of ~ 8 , suggesting that the inclusion of extra parameters in models 5_I and 6_I is superfluous. Thus despite the indifference shown by the evidence the Bayesian complexity has successfully, and correctly, relegated these models.

8 CONCLUSIONS

In this paper we have attempted to fit an optimal degree of structure to the primordial power spectrum using Bayesian model selection tools as our discriminant criteria. We find that a scale invariant spectrum is significantly ruled out, the data instead favouring a tilted spectrum, with perhaps some slight scale dependence of n_s located close to $k \sim 0.01 \text{ Mpc}^{-1}$. We fail to find any support in the data for further features beyond this simple scenario, the optimal reconstruction fitting between just two and three parameters. Previous authors (including ourselves) have regularly used many more degrees of freedom, finding a number of ‘interesting’ features in the process. In this analysis, by accounting for Occam’s razor we have found no statistically significant structure, much beyond a simple tilt, and there is, we feel, limited point in attempting more complex models at present, as the data simply cannot support them.

ACKNOWLEDGEMENTS

This work was carried out largely on the Cambridge High Performance Computing Cluster, DARWIN and we thank Stuart Rankin for assistance. We thank Roberto Trotta for extremely helpful discussions. FF is supported by fellowships from the Cambridge Commonwealth Trust and the Pakistan Higher Education Commission. MB is supported by STFC.

REFERENCES

- Barriga J., Gaztañaga E., Santos M. G., Sarkar S., 2001, MNRAS, 324, 977
- Bridges M., Lasenby A. N., Hobson M. P., 2006, MNRAS, 369, 1123
- Bridges M., Lasenby A. N., Hobson M. P., 2007, MNRAS, 381, 68
- Bridle S. L., Lewis A. M., Weller J., Efstathiou G., 2003, MNRAS, 342, L72

- CBI Supplementary Data 2004,
<http://www.astro.caltech.edu/tjp/CBI/data2004/index.html>
- Cole S., et al., 2005, MNRAS, 362, 505
- de Oliveira-Costa A., Tegmark M., Zaldarriaga M., Hamilton A., 2004, Phys.Rev.D, 69, 063516
- Dunkley J., et al., 2008, ArXiv e-prints, 0803.0586
- Easther R., Peiris H. V., 2006, Journal of Cosmology and Astro-Particle Physics, 9, 10
- Efstathiou G., 2003a, MNRAS, 343, L95
- Efstathiou G., 2003b, MNRAS, 346, L26
- Feroz F., Hobson M. P., 2008, MNRAS, 384, 449
- Feroz F., Hobson M. P., Bridges M., 2008, ArXiv e-prints, 0809.3437
- Hinshaw G., et al., 2008, ArXiv e-prints, 0803.0732
- Hobson M. P., Bridle S. L., Lahav O., 2002, MNRAS, 335, 377
- Jeffreys H., 1961, Theory of Probability. Oxford University Press
- Jones W. C., et al., 2006, ApJ, 647, 823
- Komatsu E., et al., 2008, ArXiv e-prints, 0803.0547
- Kunz M., Trotta R., Parkinson D. R., 2006, Phys.Rev.D, 74, 023503
- Leach S. M., Liddle A. R., Martin J., Schwarz D. J., 2002, Phys.Rev.D, 66, 023515
- McDonald P., et al., 2006, ApJS, 163, 80
- Marshall P., Rajguru N., Slosar A., 2006, Phys.Rev.D, 73, 067302
- Montroy T. E., et al., 2006, ApJ, 647, 813
- Mukherjee P., Wang Y., 2003, ApJ, 599, 1
- Nicholson G., Contaldi C. R., 2008, JCAP, 1, 2
- Peiris H. V., Easther R., 2006, JCAP, 10, 17
- Piacentini F., et al., 2006, ApJ, 647, 833
- Readhead A. C. S., et al., 2004, ApJ, 609, 498
- Reichardt C. L., et al., 2008, ArXiv e-prints, 0801.1491
- Sealfon C., Verde L., Jimenez R., 2005, Phys.Rev.D, 72, 103520
- Seljak U., Slosar A., McDonald P., 2006, JCAP, 10, 14
- Shafieloo A., Souradeep T., 2004, Phys.Rev.D, 70, 043523
- Skilling J., 2004, Nested Sampling for General Bayesian Computation. <http://www.inference.phy.cam.ac.uk/bayesys>
- Spergel D. N., et al. 2007, ApJS, 170, 377
- Spergel D. N., et al., 2003, ApJS, 148, 175
- Spiegelhalter D. J., Best N. G., Carlin B. P., van der Linde A., 2002, J. R. Statist. Soc. B, 64, 583
- Tegmark M., de Oliveira-Costa A., Hamilton A. J., 2003, Phys.Rev.D, 68, 123523
- Tegmark M., et al., 2004, ApJ, 606, 702
- Tegmark M., et al., 2006, Phys.Rev.D, D74, 123507
- Tocchini-Valentini D., Douspis M., Silk J., 2005, MNRAS, 359, 31
- Trotta R., 2007, MNRAS, 378, 72
- Verde L., et al., 2003, ApJS, 148, 195
- Verde L., Peiris H., 2008, JCAP, 7, 9
- Viel M., Haehnelt M. G., Lewis A., 2006, MNRAS, 370, L51